IOPscience iopscience.iop.org

Home Search Collections Journals About Contact us My IOPscience

The effect of an intense terahertz irradiation on electron transport in two-dimensional semiconductors

This article has been downloaded from IOPscience. Please scroll down to see the full text article.

1998 J. Phys.: Condens. Matter 10 3201

(http://iopscience.iop.org/0953-8984/10/14/009)

View the table of contents for this issue, or go to the journal homepage for more

Download details:
IP Address: 171.66.16.209
The article was downloaded on 14/05/2010 at 12:54

Please note that terms and conditions apply.

J. Phys.: Condens. Matter **10** (1998) 3201–3212. Printed in the UK PII: S0953-8984(98)89908-6

The effect of an intense terahertz irradiation on electron transport in two-dimensional semiconductors

X L Lei

China Centre of Advanced Science and Technology (World Laboratory), PO Box 8730, Beijing 100080, People's Republic of China, and State Key Laboratory of Functional Materials for Informatics, Shanghai Institute of Metallurgy, Chinese Academy of Sciences, 865 Changning Road, Shanghai 200050, People's Republic of China

Received 9 December 1997

Abstract. We study theoretically the electron transport in GaAs-based quasi-two-dimensional systems under the influence of an intense terahertz electromagnetic irradiation, using a balance equation approach in which the slowly varying part of the centre-of-mass velocity is distinguished from the rapidly oscillating part of it. Electron scatterings by charged impurities, and acoustic and polar optical phonons are considered and up to as many as $|n| = 60$ multiphoton channels are taken into account. The carrier mobility and the electron temperature of a typical GaAs quantum well system are calculated in the limit of small dc drift velocity (small dc field) as functions of the radiation-field strength for various frequencies in the range from 1 to 10 THz at lattice temperature $T = 10$, 77, 150 and 300 K. We find that at low lattice temperature ($T = 10$ K), dc mobility decreases monotonically with increasing strength of the radiation field, and lower frequency generally has a stronger effect in suppressing the mobility, in agreement with the experimental observation. At room temperature, on the other hand, the present theory predicts an enhancement of the dc mobility due to irradiation with a THz field.

1. Introduction

With the development of the free-electron laser, which provides a tunable source of linearly polarized far-infrared or terahertz electromagnetic radiation of high intensity, the nonlinear dynamics of low-dimensional electron gas driven by an intense terahertz (THz) electric field has become a central focus of many experimental and theoretical studies in the literature [1–6]. Among many interesting phenomena that have been reported, the effect of an intense THz irradiation on electron transport in two-dimensional (2D) semiconductors has attracted much attention. Asmar *et al* [1, 2] carried out a series of transport and optical measurements on GaAs/AlGaAs heterojunctions and quantum wells under an intense THz drive at low temperatures. They found that the dc ohmic conductivity of these quasi-2D systems is strongly suppressed by irradiation with an intense high-frequency electromagnetic field, and its behaviour is sensitively dependent on the frequency and the amplitude of the radiation. This suppression of the dc conductivity in quasi-2D systems has been attributed solely to the rise of the electron temperature caused by the illumination with the intense radiation field of THz frequency. A recent theoretical investigation [6], which takes account of other nonlinear effects of the oscillatory THz field in addition to the increase of the electron temperature by directly solving the time-dependent momentum and energy-balance equations to obtain the steady oscillating response of the drift velocity and the electron temperature to the time-dependent sinusoidal field, predicted both a dc-current suppression and an

0953-8984/98/143201+12\$19.50 © 1998 IOP Publishing Ltd

electron temperature enhancement at low temperatures, in agreement with the experiments. These low-temperature results, though quantitatively different from those derived from the carrier temperature model, do not clearly exclude the possibility that the decrease of the dc conductivity stems mainly from the rise of the electron temperature.

The purpose of the present paper is to investigate the effect of an intense terahertz irradiation on electron transport in two-dimensional semiconductors over a wider lattice temperature region: from liquid helium to room temperature.

Although the balance equation method [7–9] used in reference [6] is a reliable method for investigating the system response to a high-frequency electric field, It is rather time consuming to calculate the effect of an intense THz field on the dc transport, because one has to follow the time evolution of the applied THz field from the initial state to the steady oscillatory state before obtaining any result under the influence of a THz irradiation. Therefore we will use a different balance equation approach, which allows one to calculate the effect of a THz field of arbitrary strength on the dc transport of a 2D system based on a set of time-independent rather than time-dependent equations, and thus is more convenient for carrying out systematic analysis.

Our theoretical results show that at low lattice temperature ($T = 10$ K), dc mobility decreases monotonically with increasing strength of the radiation field, and lower frequency generally has a stronger effect in suppressing the mobility, in agreement with the experimental observation. At room temperature, on the other hand, the present theory predicts a significant enhancement of the dc mobility due to the irradiation with a THz field—quite different from the low-temperature results. This provides a feasible way to test the theory experimentally.

2. 2D centre-of-mass and relative-electron variables

We consider N_s electrons in a quasi-2D system, such as a GaAs/AlGaAs heterojunction or a quantum well, in which electrons are subjected to a confining potential $V(z)$ in the z-direction but are free to move in the x–y plane. The Hamiltonian of the electron system is written as

$$H_e = \sum_j \left[\frac{\boldsymbol{p}_{j\|}^2}{2m} + \frac{p_{jz}^2}{2m_z} + V(z_j) \right] + \sum_{i<j} V_c(\boldsymbol{r}_{i\|} - \boldsymbol{r}_{j\|}, z_i, z_j) \tag{1}$$

where $\boldsymbol{p}_{j\|} \equiv (p_{jx}, p_{jy})$ and $\boldsymbol{r}_{j\|} \equiv (x_j, y_j)$ are the momentum and coordinate of the jth electron in the 2D plane, and p_{jz} and z_j are those perpendicular to the plane; m and m_z are, respectively, the effective mass parallel and perpendicular to the plane; the last term represents the electron–electron interaction.

Assuming that a uniform dc (or slowly varying) electric field $\boldsymbol{E}_0$ and a uniform sinusoidal radiation field of frequency ω and amplitude $\boldsymbol{E}_\omega$:

$$\boldsymbol{E}(t) = \boldsymbol{E}_0 + \boldsymbol{E}_\omega \sin(\omega t) \tag{2}$$

(both $\boldsymbol{E}_0$ and $\boldsymbol{E}_\omega$ being of arbitrary strength) are applied in the 2D plane, we describe this electric field by means of a vector potential $\boldsymbol{A}(t)$ and a scalar potential $\varphi(\boldsymbol{r})$ of the form

$$\boldsymbol{A}(t) = (\boldsymbol{E}_\omega/\omega)\cos(\omega t) \tag{3}$$

$$\varphi(\boldsymbol{r}) = -\boldsymbol{r} \cdot \boldsymbol{E}_0. \tag{4}$$

In the presence of such an electric field the Hamiltonian of the system becomes

$$H_{eE} = \sum_j \left[\frac{1}{2m}(\boldsymbol{p}_{j\|} - e\boldsymbol{A}(t))^2 + \varphi(\boldsymbol{r}_{j\|}) + \frac{p_{jz}^2}{2m_z} + V(z_j) \right] + \sum_{i<j} V_c(\boldsymbol{r}_{i\|} - \boldsymbol{r}_{j\|}, z_i, z_j). \tag{5}$$

Since the z-direction motion is not affected by the field, we only need to separate the centre-of-mass motion from the relative motion in the x–y plane by introducing 2D centre-of-mass momentum and coordinate variables $\boldsymbol{P} = (P_x, P_y)$ and $\boldsymbol{R} = (X, Y)$ [7, 8]:

$$\boldsymbol{P} = \sum_j \boldsymbol{p}_{j\|} \qquad \boldsymbol{R} = \frac{1}{N_s} \sum_j \boldsymbol{r}_{j\|} \tag{6}$$

and the relative-electron momentum and coordinate variables $\boldsymbol{p}'_j = (\boldsymbol{p}'_{j\|}, p_{jz})$ and $\boldsymbol{r}' = (\boldsymbol{r}'_{j\|}, z_j)$ $(j = 1, \ldots N)$, with

$$\boldsymbol{p}'_{j\|} = \boldsymbol{p}_{j\|} - \frac{1}{N_s}\boldsymbol{P} \qquad \boldsymbol{r}'_{j\|} = \boldsymbol{r}_{j\|} - \boldsymbol{R}. \tag{7}$$

In terms of these variables, the Hamiltonian can be written as the sum of the centre-of-mass part H_{CM} and a relative-electron part H_{er}:

$$\begin{aligned} H_{\mathrm{eE}} &= H_{\mathrm{CM}} + H_{\mathrm{er}} \\ H_{\mathrm{CM}} &= \frac{\boldsymbol{P}^2}{2N_s m} - \boldsymbol{P}\cdot\boldsymbol{v}_\omega \cos(\omega t) - N_s e\boldsymbol{E}_0\cdot\boldsymbol{R} + \frac{N_s e^2}{m}\boldsymbol{A}^2(t) \end{aligned} \tag{8}$$

with

$$\boldsymbol{v}_\omega \equiv e\boldsymbol{E}_\omega/(m\omega) \tag{9}$$

and

$$H_{\mathrm{er}} = \sum_j \left[\frac{(\boldsymbol{p}'_{j\|})^2}{2m} + \frac{p_{jz}^2}{2m_z} + V(z_j) \right] + \sum_{i<j} V_c(\boldsymbol{r}'_{i\|} - \boldsymbol{r}'_{j\|}, z_i, z_j). \tag{10}$$

This relative-electron Hamiltonian is the same as that of equation (1) for the original electron system with reference to the lattice, and thus can be written in the second-quantization representation as

$$H_{\mathrm{er}} = \sum_{s,\boldsymbol{k}_\|,\sigma} \varepsilon_s(\boldsymbol{k}_\|) c^\dagger_{s\boldsymbol{k}_\|\sigma} c_{s\boldsymbol{k}_\|\sigma} + \frac{1}{2} \sum_{\substack{\boldsymbol{k}_\|,\boldsymbol{k}'_\|,\boldsymbol{q}_\|,\sigma,\sigma' \\ \iota',\iota,s',s}} V_{\iota',\iota,s',s}(q_\|) c^\dagger_{\iota'\boldsymbol{k}_\|+\boldsymbol{q}_\|\sigma} c^\dagger_{s'\boldsymbol{k}'_\|-\boldsymbol{q}_\|\sigma'} c_{s\boldsymbol{k}'_\|\sigma'} c_{\iota\boldsymbol{k}_\|\sigma}. \tag{11}$$

Here $c^\dagger_{s\boldsymbol{k}_\|\sigma}$ $(c_{s\boldsymbol{k}_\|\sigma})$ are creation (annihilation) operators of the relative electrons. We have used the single-electron state in the absence of the Coulomb interaction as the basis for the second-quantization representation, which is designated by a subband index s and a 2D wavevector $\boldsymbol{k}_\|$ with the energy

$$\varepsilon_s(\boldsymbol{k}_\|) = \varepsilon_s + \frac{k_\|^2}{2m} \tag{12}$$

and wave function

$$\psi_{s\boldsymbol{k}_\|}(\boldsymbol{r}, z) = \mathrm{e}^{\mathrm{i}\boldsymbol{k}_\|\cdot\boldsymbol{r}} \zeta_s(z) \tag{13}$$

where $\zeta_s(z)$ is the envelope function. We assume that the system has area unity in the x–y plane. The expression for $V_{\iota',\iota,s',s}(q_\|)$ is given in reference [8]. At the same time, the electron–impurity and electron–phonon interactions, H_{ei} and H_{ep}, can also be written in terms of the centre-of-mass coordinate $\boldsymbol{R}$ and the creation and annihilation operators of the relative electrons [7].

3. Force and energy-balance equations for quasi-2D systems

With the help of the total Hamiltonian of the electron–phonon system,

$$H = H_{\rm CM} + H_{\rm er} + H_{\rm ei} + H_{\rm ep} + H_{\rm ph}$$

($H_{\rm ph}$ stands for the phonon Hamiltonian), we can calculate the rates of change of the CM coordinate $\boldsymbol{R}$, the CM momentum $\boldsymbol{P}$ and the relative-electron energy $H_{\rm er}$ on the basis of the Heisenberg equation of motion. In particular, the rate of change of the CM coordinate $\boldsymbol{R}$, which is the CM velocity $\boldsymbol{V}$, is given by

$$\boldsymbol{V} \equiv \dot{\boldsymbol{R}} = -{\rm i}[\boldsymbol{R}, H] = \frac{\boldsymbol{P}}{N_{\rm s}m} - \boldsymbol{v}_\omega \cos(\omega t) \tag{14}$$

containing a rapid oscillatory term induced by the radiation field.

Following reference [7], in view of the enormous mass of the CM, we can treat the CM coordinate $\boldsymbol{R}$ and velocity $\boldsymbol{V}$ classically, and by neglecting their small fluctuations we will regard them as time-dependent expectation (or average) values of the CM coordinate and velocity, $\boldsymbol{R}(t)$ and $\boldsymbol{V}(t)$. Furthermore, the CM will not be able to follow the rapid oscillation of the radiation field if its frequency is high enough. Therefore, in the gauge used, the statistical average of the CM momentum can be regarded as a slowly varying quantity

$$\left\langle \frac{\boldsymbol{P}}{N_{\rm s}m} \right\rangle = \boldsymbol{v}_0 \tag{15}$$

which is identified as the average velocity of the CM, or the average drift velocity of the carrier system. Thus we write

$$\boldsymbol{V}(t) = \boldsymbol{v}_0 - \boldsymbol{v}_\omega \cos(\omega t) \tag{16}$$

and

$$\boldsymbol{R}(t) = \int_{t_0}^{t} \boldsymbol{V}(s)\ {\rm d}s + \boldsymbol{R}(t_0). \tag{17}$$

This indicates that the interaction $H_{\rm ei} + H_{\rm ep}$, the rate of change of the CM momentum, $-{\rm i}[\boldsymbol{P}, H]$, and the rate of change of the relative-electron energy, $-{\rm i}[H_{\rm er}, H]$, are time-dependent operators in the relative-electron–phonon systems through their dependence on the CM coordinate $\boldsymbol{R}(t)$. In the presence of a uniform high-frequency radiation field, the relative-electron–phonon system turns out to be the same as that discussed in reference [8] for the case without the radiation field ($E_\omega = 0$), and thus we can proceed in exactly the same way as in reference [8]. For 2D systems having electron sheet density of the order of, or higher than, 10^{15} m^{-2}, the intrasubband and intersubband Coulomb interaction are sufficiently strong that it is adequate to describe their transport state using a single electron temperature T_e and a common chemical potential for all of the subbands. Therefore the density matrix of the relative-electron–phonon system can be solved from the Liouville equation by starting from an initial state at time $t = -\infty$, in which the phonon system is in equilibrium at the lattice temperature T and the relative-electron system is in equilibrium at an electron temperature T_e:

$$\hat{\rho}|_{t=-\infty} = \hat{\rho}_0 = \frac{1}{Z} {\rm e}^{-H_{\rm er}/T_e} {\rm e}^{H_{\rm ph}/T}. \tag{18}$$

With the density matrix thus obtained to the first order in $H_{\rm ei} + H_{\rm ep}$, we can derive the momentum-balance equation by taking the statistical average of the operator equation

$\dot{\boldsymbol{P}} = -\mathrm{i}[\boldsymbol{P}, H]$ and identifying $\dot{\boldsymbol{P}}$ as $N_\mathrm{s} m (\mathrm{d}\boldsymbol{v}_0/\mathrm{d}t)$. We have

$$Nm \frac{\mathrm{d}}{\mathrm{d}t}\boldsymbol{v}_0 = Ne\boldsymbol{E}_0 + \boldsymbol{F}_i + \boldsymbol{F}_p. \tag{19}$$

The frictional forces $\boldsymbol{F}_i$ and $\boldsymbol{F}_p$, due to impurity and phonon scatterings, are given respectively by

$$\boldsymbol{F}_i = \sum_{s',s,\boldsymbol{q}_\parallel} \boldsymbol{q}_\parallel |U_{s's}(\boldsymbol{q}_\parallel)|^2 \int_{-\infty}^{t} \mathrm{d}t' \, \exp\left[\mathrm{i}\boldsymbol{q}_\parallel \cdot \int_{t'}^{t} \boldsymbol{V}(\tau)\, \mathrm{d}\tau\right] \times \sum_{\boldsymbol{k}_\parallel,\sigma} \left\langle \left[c^\dagger_{s'\boldsymbol{k}_\parallel+\boldsymbol{q}_\parallel\sigma}(t-t') c_{s\boldsymbol{k}_\parallel\sigma}(t-t'), c^\dagger_{s\boldsymbol{k}_\parallel\sigma} c^\dagger_{s'\boldsymbol{k}_\parallel+\boldsymbol{q}_\parallel\sigma} \right] \right\rangle_0. \tag{20}$$

$$\boldsymbol{F}_p = 2 \sum_{s',s,\boldsymbol{q},\lambda} \boldsymbol{q}_\parallel |M_{s's}(\boldsymbol{q},\lambda)|^2 \int_{-\infty}^{t} \mathrm{d}t' \, \exp\left[\mathrm{i}\boldsymbol{q}_\parallel \cdot \int_{t'}^{t} \boldsymbol{V}(\tau)\, \mathrm{d}\tau\right] \times \sum_{\boldsymbol{k}_\parallel,\sigma} \left\langle \left[\phi_{\boldsymbol{q}\lambda}(t-t') c^\dagger_{s'\boldsymbol{k}_\parallel+\boldsymbol{q}_\parallel\sigma}(t-t') c_{s\boldsymbol{k}_\parallel\sigma}(t-t'), \phi_{-\boldsymbol{q}\lambda} c^\dagger_{s\boldsymbol{k}_\parallel\sigma} c^\dagger_{s'\boldsymbol{k}_\parallel+\boldsymbol{q}_\parallel\sigma} \right] \right\rangle_0. \tag{21}$$

Here, the statistical averaging is performed with respect to the initial density matrix ρ_0 given by equation (18), $U_{s's}(\boldsymbol{q}_\parallel)$ is an effective impurity potential, and $M_{s's}(\boldsymbol{q},\lambda)$ is the electron–phonon matrix element (with the 3D phonon model) related to subbands s' and s. Their explicit expressions were given in reference [8].

With the velocity function given by equation (16), the exponential factor in the above equations becomes

$$\exp\left[\mathrm{i}\boldsymbol{q}_\parallel \cdot \int_{t'}^{t} \boldsymbol{V}(\tau)\, \mathrm{d}\tau\right] = \exp\left[\mathrm{i}\boldsymbol{q}_\parallel \cdot \boldsymbol{v}_0(t-t')\right] \exp\left[-\mathrm{i}\boldsymbol{q}_\parallel \cdot \boldsymbol{r}_\omega(\sin(\omega t) - \sin(\omega t'))\right] \tag{22}$$

with

$$\boldsymbol{r}_\omega \equiv \boldsymbol{v}_\omega/\omega = e\boldsymbol{E}_\omega/(m\omega^2). \tag{23}$$

Using the equality related to the Bessel functions,

$$\mathrm{e}^{-\mathrm{i}z\sin x} = \sum_{n=-\infty}^{\infty} J_n(z)\mathrm{e}^{-\mathrm{i}nx}$$

we can rewrite the exponential factor in equations (20) and (21) as a sum of two terms:

$$\sum_{n=-\infty}^{\infty} J_n^2(\boldsymbol{q}_\parallel \cdot \boldsymbol{r}_\omega) \mathrm{e}^{\mathrm{i}\boldsymbol{q}_\parallel\cdot\boldsymbol{v}_0(t-t')} \mathrm{e}^{-\mathrm{i}n\omega(t-t')} + \sum_{m\neq 0} \mathrm{e}^{-\mathrm{i}m\omega t} \left[\sum_{n=-\infty}^{\infty} J_n(\boldsymbol{q}_\parallel \cdot \boldsymbol{r}_\omega) J_{n-m}(\boldsymbol{q}_\parallel \cdot \boldsymbol{r}_\omega) \mathrm{e}^{\mathrm{i}\boldsymbol{q}_\parallel\cdot\boldsymbol{v}_0(t-t')} \mathrm{e}^{-\mathrm{i}n\omega(t-t')} \right]. \tag{24}$$

After the integration over t', the first term yields a contribution no longer dependent on t, while the second term is rapidly oscillating at the fundamental frequency ω and its harmonics. If what one measures is an average over a time interval much longer than the period of the radiation field, the contribution of the second term is not detectable. Therefore we are left with

$$\boldsymbol{F}_i = \sum_{s',s,\boldsymbol{q}_\parallel} \boldsymbol{q}_\parallel |U_{s's}(\boldsymbol{q}_\parallel)|^2 \sum_{n=-\infty}^{\infty} J_n^2(\boldsymbol{q}_\parallel \cdot \boldsymbol{r}_\omega) \Pi_2(s', s, \boldsymbol{q}_\parallel, \omega_0 - n\omega) \tag{25}$$

$$\boldsymbol{F}_p = 2\sum_{s',s,\boldsymbol{q},\lambda} \boldsymbol{q}_\parallel |M_{s's}(\boldsymbol{q},\lambda)|^2 \sum_{n=-\infty}^{\infty} J_n^2(\boldsymbol{q}_\parallel \cdot \boldsymbol{r}_\omega) \times \Pi_2(s', s, \boldsymbol{q}_\parallel, \Omega_{q\lambda}+\omega_0-n\omega)\left[n\left(\frac{\Omega_{q\lambda}}{T}\right) - n\left(\frac{\Omega_{q\lambda}+\omega_0-n\omega}{T_e}\right)\right]. \tag{26}$$

Here $\omega_0 \equiv \boldsymbol{q}_\parallel \cdot \boldsymbol{v}_0$, $n(x) \equiv 1/[\exp(x)-1]$ is the Bose function, and $\Pi_2(s', s, \boldsymbol{q}_\parallel, \Omega)$ is the imaginary part of the electron density correlation function related to subbands s' and s at electron temperature T_e [8].

The energy-balance equation is obtained by taking the statistical average of the operator equation $\dot{H}_{\rm er} = -{\rm i}[H_{\rm er}, H]$ and identifying $\langle \dot{H}_e \rangle$ as the rate of change of the relative-electron energy $\mathcal{E}_e$. By the same consideration as above, we arrive at the result

$$\frac{\rm d}{{\rm d}t}\mathcal{E}_e = -\boldsymbol{v}_0 \cdot (\boldsymbol{F}_i + \boldsymbol{F}_p) - W + S_p \tag{27}$$

where

$$W = 2\sum_{s',s,\boldsymbol{q},\lambda} \Omega_{q\lambda} |M_{s's}(\boldsymbol{q},\lambda)|^2 \sum_{n=-\infty}^{\infty} J_n^2(\boldsymbol{q}_\parallel \cdot \boldsymbol{r}_\omega) \times \Pi_2(s', s, \boldsymbol{q}_\parallel, \Omega_{q\lambda}+\omega_0-n\omega)\left[n\left(\frac{\Omega_{q\lambda}}{T}\right) - n\left(\frac{\Omega_{q\lambda}+\omega_0-n\omega}{T_e}\right)\right] \tag{28}$$

is the rate of energy transfer from the electron system to the phonon system, and

$$S_p = \sum_{s',s,\boldsymbol{q}_\parallel} |U_{s's}(\boldsymbol{q}_\parallel)|^2 \sum_{n=-\infty}^{\infty} J_n^2(\boldsymbol{q}_\parallel \cdot \boldsymbol{r}_\omega) n\omega \Pi_2(s', s, \boldsymbol{q}_\parallel, \omega_0 - n\omega) + 2\sum_{s',s,\boldsymbol{q},\lambda} |M_{s's}(\boldsymbol{q},\lambda)|^2 \sum_{n=-\infty}^{\infty} J_n^2(\boldsymbol{q}_\parallel \cdot \boldsymbol{r}_\omega) n\omega \times \Pi_2(s', s, \boldsymbol{q}_\parallel, \Omega_{q\lambda}+\omega_0-n\omega)\left[n\left(\frac{\Omega_{q\lambda}}{T}\right) - n\left(\frac{\Omega_{q\lambda}+\omega_0-n\omega}{T_e}\right)\right] \tag{29}$$

is the rate of gain of the energy of the electron system from the radiation field through the multiphoton process ($n = \pm 1, \pm 2, \ldots$) in association with intraband and interband transitions of electrons. When ω is less than the energy separation of the subbands, such a transition process is possible only with the assistance of the impurity or phonon scattering.

The frictional forces $\boldsymbol{F}_i$ and $\boldsymbol{F}_p$, and the electron energy-loss rate W and energy-gain rate S_p, are functions of $\boldsymbol{v}_0$ and T_e. They also depend on the amplitude E_ω and the frequency ω of the radiation field. A radiation field affects carrier transport (i) by changing the frictional forces $\boldsymbol{F}_i$, $\boldsymbol{F}_p$ and the electron energy-loss rate W and (ii) by supplying an energy S_p to the electron system through the multiphoton process ($n = \pm 1, \pm 2, \ldots$). Even without absorption or emission of photons (zero-photon processes, i.e. $n = 0$ only), the frictional forces and the energy-loss rate are still affected by the presence of a finite radiation field $E_\omega \neq 0$.

In the case without a radiation field ($E_\omega = 0$), in view of the facts that $J_0(0) = 1$ and $J_n(0) = 0$ ($n \neq 0$) we have $S_p = 0$, and $\boldsymbol{F}$ and W reduce to the corresponding expressions of reference [8], as they should. Likewise, for very high frequency we have $J_n^2(\boldsymbol{q}_\parallel \cdot \boldsymbol{r}_\omega) \propto \omega^{-4|n|}$, leading to a vanishing S_p and the same $\boldsymbol{F}$ and W as those without a radiation field. This indicates that a very-high-frequency radiation field has no influence on intraband carrier transport. The far-infrared or THz field is the regime of the electromagnetic waves, which would strongly affect the transport behaviour of carriers in semiconductors. The momentum- and energy-balance equations derived here provide a convenient tool for analysing this effect.

4. The small-v_0 limit

For constant (dc) field $\boldsymbol{E}_0$, equations (19) and (27) apparently have a steady-state solution with constant $\boldsymbol{v}_0$ and T_e determined by the following equations:

$$N_s e\boldsymbol{E}_0 + \boldsymbol{F}_i + \boldsymbol{F}_p = 0 \tag{30}$$

$$N_s e\boldsymbol{E}_0 \cdot \boldsymbol{v}_0 - W + S_p = 0. \tag{31}$$

To determine the ohmic mobility of a quasi-2D system subjected to an intense high-frequency irradiation, we consider the small-v_0 limit of equations (30) and (31). In the limit of $\boldsymbol{v}_0 \to 0$, the energy-balance equation, equation (31), reduces to

$$\begin{aligned} 0 = S_p - W = &\sum_{s',s,\boldsymbol{q}_\parallel} |U_{s's}(\boldsymbol{q}_\parallel)|^2 \sum_{n=-\infty}^{\infty} J_n^2(q_x r_\omega) n\omega \Pi_2(s', s, \boldsymbol{q}_\parallel, -n\omega) \\ &+ 2 \sum_{s',s,\boldsymbol{q},\lambda} |M_{s's}(\boldsymbol{q}, \lambda)|^2 \sum_{n=-\infty}^{\infty} J_n^2(q_x r_\omega)(n\omega - \Omega_{\boldsymbol{q}\lambda}) \\ &\times \Pi_2(s', s, \boldsymbol{q}_\parallel, \Omega_{\boldsymbol{q}\lambda} - n\omega) \left[n\left(\frac{\Omega_{\boldsymbol{q}\lambda}}{T}\right) - n\left(\frac{\Omega_{\boldsymbol{q}\lambda} - n\omega}{T_e}\right)\right]. \end{aligned} \tag{32}$$

Here we assume that the radiation field is in the x-direction. This equation determines the electron temperature T_e, which may be greatly different from the lattice temperature T when the system is irradiated with an intense THz field even without a dc field.

The force-balance equation (30) determines the resistivity, which depends on the relative directions of $\boldsymbol{E}_0$ and $\boldsymbol{E}_\omega$. In the case of $\boldsymbol{E}_0 \| \boldsymbol{E}_\omega$ or $\boldsymbol{E}_0 \perp \boldsymbol{E}_\omega$, $\boldsymbol{v}_0$ is in the same direction as $\boldsymbol{E}_0$, and the inverse mobility, defined by $1/\mu \equiv E_0/v_0$, is given by

$$\frac{1}{\mu} = \frac{1}{\mu_i} + \frac{1}{\mu_p} \tag{33}$$

$$\frac{1}{\mu_i} = \frac{1}{N_s e} \sum_{s',s,\boldsymbol{q}_\parallel} q_\alpha^2 |U_{s's}(\boldsymbol{q}_\parallel)|^2 \sum_{n=-\infty}^{\infty} J_n^2(q_x r_\omega) \left[\frac{\partial}{\partial\Omega} \Pi_2(s', s, \boldsymbol{q}_\parallel, \Omega)\right]_{\Omega=n\omega} \tag{34}$$

$$\begin{aligned} \frac{1}{\mu_p} = \frac{2}{N_s e} &\sum_{s',s,\boldsymbol{q},\lambda} q_\alpha^2 |M_{s's}(\boldsymbol{q}, \lambda)|^2 \sum_{n=-\infty}^{\infty} J_n^2(q_x r_\omega) \left\{ \Pi_2(s', s, \boldsymbol{q}_\parallel, \Omega_{\boldsymbol{q}\lambda} - n\omega) \left[\frac{1}{T_e} n'\left(\frac{\Omega_{\boldsymbol{q}\lambda}}{T_e}\right)\right] \right. \\ &\left. + \left[n\left(\frac{\Omega_{\boldsymbol{q}\lambda} - n\omega}{T_e}\right) - n\left(\frac{\Omega_{\boldsymbol{q}\lambda}}{T}\right)\right] \left[\frac{\partial}{\partial\Omega} \Pi_2(s', s, \boldsymbol{q}_\parallel, \Omega)\right]_{\omega=\Omega_{\boldsymbol{q}\lambda} - n\omega} \right\}. \end{aligned} \tag{35}$$

Here $\alpha = x$ or y for the parallel ($\boldsymbol{E}_0 \| \boldsymbol{E}_\omega$) or perpendicular ($\boldsymbol{E}_0 \perp \boldsymbol{E}_\omega$) configuration.

5. Numerical results

We have calculated the electron temperature T_e and mobility $1/\mu$ in the small-v_0 limit at lattice temperatures $T = 10, 77, 150$ and 300 K in a GaAs-based quantum well having the well width $a = 12.5$ nm, electron sheet density $N_s = 5.5 \times 10^{15}$ m^{-2} and low-temperature (4.2 K) linear mobility $\mu_0 = 31$ m^2 V^{-1} s^{-1}, subjected to a radiation field of various frequencies and amplitudes.

We consider both the electron–polar-optical-phonon scattering (via the Fröhlich coupling) and the electron–acoustic-phonon scattering (via the deformation potential and the piezoelectric couplings), as well as the elastic scattering, which is assumed to be due to the remote charged impurities located at a distance of 40 nm from the centre plane of

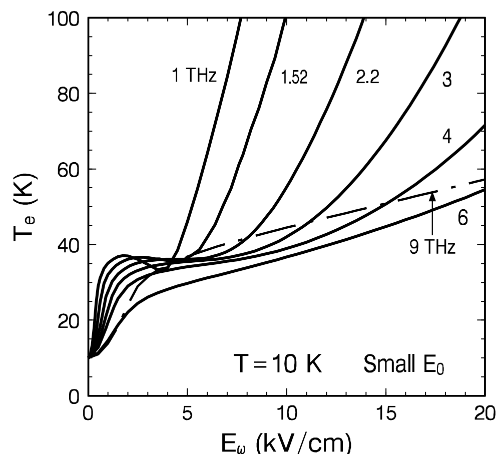

Figure 1. The calculated electron temperature T_e is shown as a function of the strength E_ω of the radiation field having frequency $\omega/2\pi = 1, 1.52, 2.2, 3, 4, 6$ and 9 THz, in the small-dc-field limit $E_0 \sim 0$ at lattice temperature $T = 10$ K.

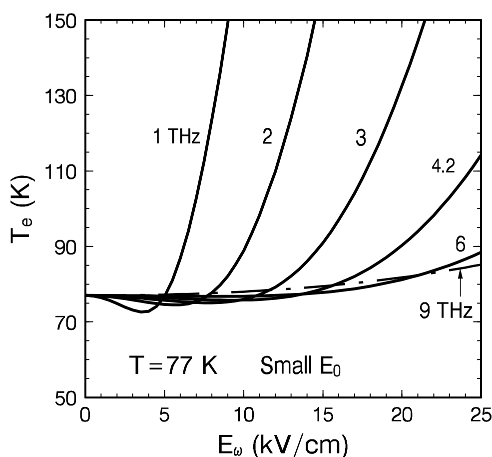

Figure 2. The calculated electron temperature T_e is shown as a function of the strength E_ω of the radiation field having frequency $\omega/2\pi = 1, 2, 3, 4.2, 6$ and 9 THz, in the small-dc-field limit $E_0 \sim 0$ at lattice temperature $T = 77$ K.

the well. The phonons are assumed to be the same as those of bulk GaAs and to remain in equilibrium at the lattice temperature T during the transport process. We consider the role of the two lowest subbands ($s = 0, 1$). The energy separation between the bottoms of the zeroth and the first subbands, $\varepsilon_{10} \equiv \varepsilon_1 - \varepsilon_0$, is taken to be 69 meV. For simplicity, the form factors are calculated using the corresponding subband functions of an infinitely deep potential well having the same well width. The other material parameters of bulk GaAs used in the calculation are listed in table 1 (m_e stands for the free-electron mass).

In the numerical calculation we have included contributions from as many optical channels as are needed. The larger the amplitude E_ω or the lower the frequency ω of the radiation field, the more optical channels have to be included to give sufficient accuracy. A maximum of $|n| = 0, 1, \ldots, 60$ has been taken in obtaining the results presented

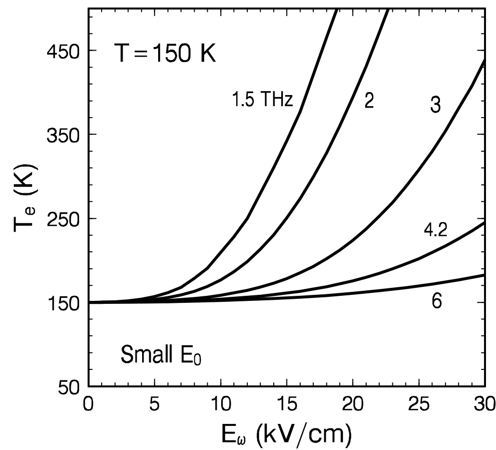

Figure 3. The calculated electron temperature T_e is shown as a function of the strength E_ω of the radiation field having frequency $\omega/2\pi = 1.5, 2, 3, 4.2$ and 6 THz, in the small-dc-field limit $E_0 \sim 0$ at lattice temperature $T = 150$ K.

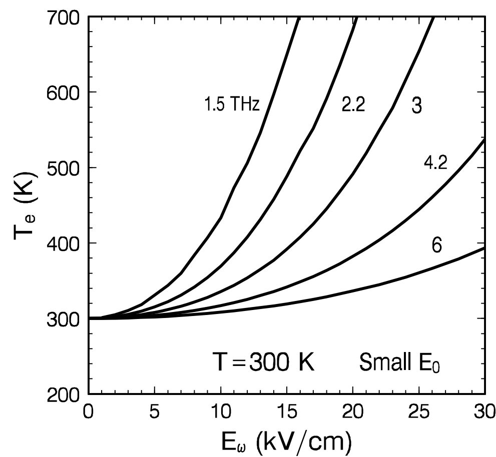

Figure 4. The calculated electron temperature T_e is shown as a function of the strength E_ω of the radiation field having frequency $\omega/2\pi = 1.5, 2.2, 3, 4.2$ and 6 THz, in the small-dc-field limit $E_0 \sim 0$ at lattice temperature $T = 300$ K.

in this section.

Figures 1–4 show the electron temperature T_e as a function of the radiation-field strength E_ω for several different frequencies $\omega/2\pi$ from 1 to 9 THz in the parallel configuration at lattice temperature $T = 10, 77, 150$ and 300 K, respectively. At $T = 10$ K, T_e grows rapidly with E_ω increasing from zero, and shows a minimum for lower frequencies (1–3 THz) before its monotonic rise with rising E_ω. At $T = 77$ K, the initial rising of T_e disappears but minima remain, exhibiting electron temperature cooling (T_e is lower than T) within a certain range of E_ω for frequency $\omega/2\pi = 1, 2, 3$ and 4 THz. At higher temperatures ($T = 150$ and 300 K) all of these features disappear and for a given frequency T_e grows with increasing E_ω monotonically.

With these T_e-values, the mobility of the quantum well system irradiated with a

Table 1. Parameters for GaAs.

Parameter	Unit	Value
Material mass density d	g cm^{-3}	5.31
Effective electron edge-band mass m	m_e	0.067
Optical dielectric constant κ_∞	1	10.8
Low-frequency dielectric constant κ	1	12.9
Transverse sound velocity v_{st}	m s^{-1}	2.48×10^3
Longitudinal sound velocity v_{sl}	m s^{-1}	5.29×10^3
Longitudinal-optical-phonon energy Ω_{LO}	meV	35.4
Acoustic deformation potential Ξ	eV	8.5
Piezoelectric constant e_{14}	V s^{-1}	1.41×10^9

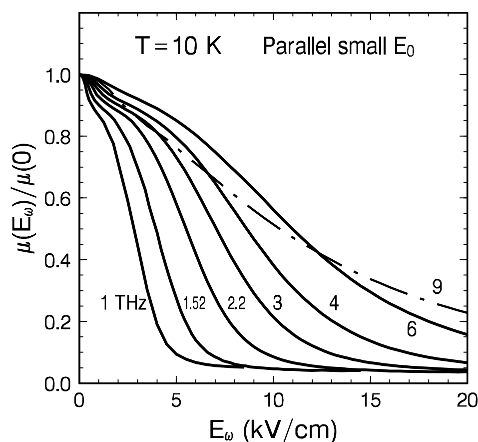

Figure 5. The normalized mobility $\mu(E_\omega)/\mu(0)$ at lattice temperature $T = 10$ K, in the small-dc-field limit $E_0 \sim 0$ in the parallel configuration, is shown as a function of the radiation-field strength E_ω having frequency $\omega/2\pi = 1, 1.52, 2.2, 3, 4, 6$ and 9 THz.

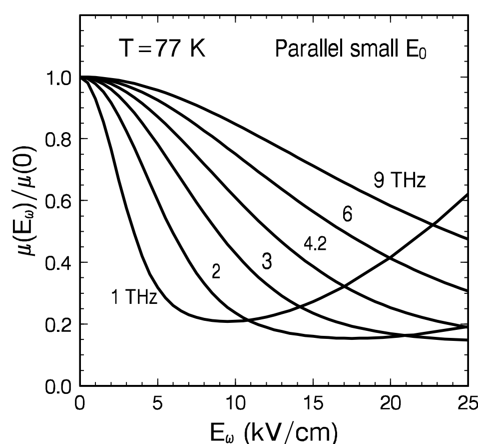

Figure 6. The normalized mobility $\mu(E_\omega)/\mu(0)$ at lattice temperature $T = 77$ K, in the small-dc-field limit $E_0 \sim 0$ in the parallel configuration, is shown as a function of the radiation-field strength E_ω having frequency $\omega/2\pi = 1, 2, 3, 4.2, 6$ and 9 THz.

THz field of strength E_ω, $\mu(E_\omega)$, is obtained from formulae (33)–(35). Figures 5–8 show the calculated mobility $\mu(E_\omega)$ normalized with respect to its value in the absence of the radiation field ($E_\omega = 0$), $\mu(0)$, as a function of the radiation-field strength E_ω for several different frequencies $\omega/2\pi$ from 1 to 9 THz in the parallel configuration at lattice temperature $T = 10, 77, 150$ and 300 K, respectively. At low lattice temperature ($T = 10$ K), $\mu(E_\omega)/\mu(0)$ monotonically decreases with increasing E_ω for a fixed frequency. Lower frequency generally has a stronger effect than higher frequency. $\mu(E_\omega)$ can be suppressed by the radiation field down to about 0.05 $\mu(0)$. When lattice temperature increases ($T = 77$ K), a minimum in the $\mu(E_\omega)/\mu(0)$ against E_ω curve shows up at lower frequency. At $\omega/2\pi = 1$ THz, $\mu(E_\omega)/\mu(0)$ reaches a minimum of 0.2 at around $E_\omega = 9.5$ kV cm^{-1} before increasing with increasing E_ω. With further increased lattice temperature ($T = 150$ K), at $\omega/2\pi = 1.5$ THz this $\mu(E_\omega)/\mu(0)$ reaches a minimum of only 0.65 at around $E_\omega = 8.5$ kV cm^{-1} and then rapidly increases. At room temperature, $T = 300$ K, the behaviour of $\mu(E_\omega)/\mu(0)$ is almost completely reversed in comparison with that at $T = 10$ K: instead of decreasing, the calculated $\mu(E_\omega)/\mu(0)$ essentially increases with increasing E_ω. Only for high frequencies (2.2, 3, 4.2 and 6 THz) does $\mu(E_\omega)/\mu(0)$

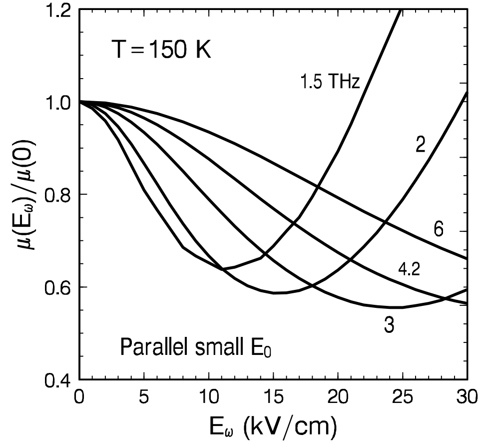

Figure 7. The normalized mobility $\mu(E_\omega)/\mu(0)$ at lattice temperature $T = 150$ K, in the small-dc-field limit $E_0 \sim 0$ in the parallel configuration, is shown as a function of the radiation-field strength E_ω having frequency $\omega/2\pi = 1.5, 2, 3, 4.2$ and 6 THz.

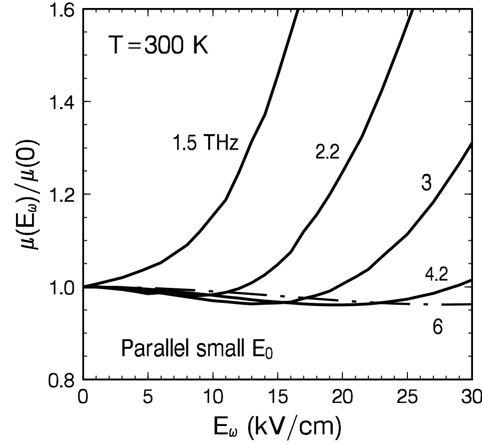

Figure 8. The normalized mobility $\mu(E_\omega)/\mu(0)$ at lattice temperature $T = 300$ K, in the small-dc-field limit $E_0 \sim 0$ in the parallel configuration, is shown as a function of the radiation-field strength E_ω having frequency $\omega/2\pi = 1.5, 2.2, 3, 4.2$ and 6 THz.

show a slight decrease with initial growth of E_ω. At $\omega/2\pi = 1.5$ THz, $\mu(E_\omega)/\mu(0)$ immediately increases with increasing E_ω from zero.

The above features can be understood by considering the role of an intense radiation field. As pointed out in section 3, a radiation field affects carrier transport (i) by changing the frictional forces $\boldsymbol{F}_i$, $\boldsymbol{F}_p$ and the electron energy-loss rate W and (ii) by supplying an energy S_p to the electron system through the zero-photon process ($n = 0$) and the multiphoton ($n \geqslant 1$) processes. With the increase of $r_\omega \equiv eE_\omega/(m\omega^2)$, i.e. the increase of the amplitude or the decrease of the frequency of the radiation field, (i) the contributions to the frictional force F and the energy-transfer rate W from the zero-photon process are weakened, but (ii) an increasing number of multiphoton processes become important in determining the carrier transport. Since the contributions to F and W from multiphoton processes are generally small due to the cancellation between the n and $-n$ terms, an increase in E_ω (or a decrease in ω) leads to a decrease in F and W if the electron temperature remains unchanged. On the other hand, the increasing number of multiphoton processes greatly enhances S_p, the rate of the energy supplied from the radiation field. This, together with the decreased W, results in the rise of the electron temperature with growing E_ω, which, in turn, enhances the frictional force, i.e. decreases the mobility. This electron-temperature-raising effect is more remarkable at lower lattice temperature than at higher lattice temperature because the main electron energy-loss mechanism (polar-optical-phonon scattering) is much less effective at low temperature. It is the interplay of these two effects that gives rise to the major numerical features: dc mobility decreases at low lattice temperature ($T = 10$ K) and increases at room temperature, while it exhibits minima at lattice temperatures in between, with increasing strength of the radiation field.

The predicted suppression of the dc current or conductivity by the irradiation with the THz field at low temperature was indeed observed experimentally in GaAs heterojunctions and quantum wells [1, 2]. Because of the lack of availability of experimental data at higher temperatures, the theoretically predicted enhancement of the dc mobility in quasi-2D systems caused by the irradiation with the THz field at room temperature cannot be compared with

measurements for the time being. We expect that the pertinent experimental data will be available in the near future.

Acknowledgments

This work was supported by the National Natural Science Foundation of China, the National and Shanghai Municipal Commissions of Science and Technology of China, and the Shanghai Foundation for Research and Development of Applied Materials.

References

[1] Asmar N G, Markelz A G, Gwinn E G, Černe J, Sherwin M S, Campman K L, Hopkins P F and Gossard A C 1995 *Phys. Rev.* B **51** 18 041
[2] Asmar N G, Černe J, Markelz A G, Gwinn E G, Sherwin M S, Campman K L and Gossard A C 1996 *Appl. Phys. Lett.* **68** 829
[3] Unterrainer K, Keay B J, Wanke M C, Allen S J, Leonard D, Medeiros-Ribeiro G, Bhattacharya U and Rodwell M J W 1996 *Phys. Rev. Lett.* **76** 2973
[4] Murdin B N, Heiss W, Langerak C J G M, Lee S-C, Galbraith I, Strasser G, Gornik E, Helm M and Pidgeon C R 1997 *Phys. Rev.* B **55** 5171
[5] Xu W and Zhang C 1997 *Phys. Rev.* B **55** 5259
[6] Lei X L, Dong B and Chen Y Q 1997 *Phys. Rev.* B **56** 12 120
[7] Lei X L and Ting C S 1985 *Phys. Rev.* B **32** 1112
[8] Lei X L, Birman J L and Ting C S 1985 *J. Appl. Phys.* **58** 2270
[9] Lei X L, Cui H L and Horing N J M 1987 *J. Phys. C: Solid State Phys.* **20** L287